JOURNAL OF APPLIED ELECTROCHEMISTRY 18 (1988) 422–430

# Study of the effect of electrode resistance on current density distribution in cylindrical electrochemical reactors

J. M. BISANG, G. KREYSA*

*Programa de Electroquimica Aplicada e Ingenieria Electroquimica (PRELINE), Facultad de Ingenueria Quimica, Universidad Nacional del Litoral, Santiago del Estero 2829, 3000 Santa Fe, Argentina*

Received 10 August 1987; revised 22 October 1987

The distribution of current density in a cylindrical electrochemical reactor was determined experimentally, a thin Pt wire, 0.2 mm diameter and 500–600 mm long, being employed as central electrode. In these investigations two methods are used: (i) a reactor with a segmented counterelectrode; in this case, measurements of the current in each ring of the counterelectrode were made; (ii) a reactor with a bi-electrode probe; in this case, the distribution was obtained by measuring the ohmic drop in the solution phase, with the probe being positioned at different heights. A mathematical model to represent such reactors was developed assuming an axially constant electrolyte potential. The experimental and theoretical values are compared in order to determine the predictive suitability of the proposed model. Both the error in predicting the feeder overvoltage and a statistical parameter ($\bar{\delta}_r$) denote the agreement between the computed and the measured current density distributions. The parameters acting upon the current distribution were lumped in a single dimensionless variable, the so-called modified Wagner number, used to determine the applicability range of the proposed model. It was concluded that when this number exceeds $15 \times 10^{-3}$, for concentrated solutions, the model can be used to design this type of reaction.

## Nomenclature

| | |
|---|---|
| $A_s$ | surface area per unit volume of electrode ($cm^{-1}$) |
| $b$ | constant defined by Equation 12 ($V^{-1}$) |
| $B$ | integration constant defined by Equation 15 |
| $E$ | error percentage |
| $E_0$ | reversible electrode potential (V) |
| $i$ | current density ($A\,cm^{-2}$) |
| $\bar{i}$ | average current density at $\Delta x$ ($A\,cm^{-2}$) |
| $i_0$ | exchange current density ($A\,cm^{-2}$) |
| $I$ | total current (A) |
| $L$ | electrode length (cm) |
| $N$ | number of experimental values in Equation 28 |
| $r$ | radius (cm) |
| $r_r$ | radial position of the reference electrode (cm) |
| $R_m$ | resistance of the metal phase ($\Omega$) |
| $R_p$ | polarization resistance ($\Omega$) |
| $RT/F$ | constant (0.0257 V at 25° C) (V) |
| $Wa^*$ | modified Wagner number |
| $x$ | axial coordinate (cm) |

*Greek characters*

| | |
|---|---|
| $\alpha_c$ | charge transfer coefficient |
| $\gamma$ | electrode effectiveness factor |
| $\bar{\delta}_r$ | parameter which evaluates the predictive ability of the model to determine current density distribution |
| $\Delta V$ | potential of the working electrode at $x = 0$ with respect to the standard hydrogen electrode including the electrolyte $iR$ drop (V) |
| $\nu_e$ | charge number of the electrode reaction |
| $\eta$ | overvoltage (V) |
| $\varrho$ | resistivity ($\Omega$ cm) |
| $\phi$ | potential (V) |

*Subscripts*

| | |
|---|---|
| e | electrode |
| exp | experimental |
| m | metal phase |
| s | solution phase |
| th | theoretical |

## 1. Introduction

In recent years many chemical industries have begun to use activated electrodes to reduce the specific energy consumption of the process, e.g. the dimensionally stable anodes for generating chlorine and oxygen, and the activated cathodes for hydrogen evolution. The electrodes are able to work at high current densities with very low overvoltages. Consequently, the resistance of the metal exerts a major influence on the

* Dechema-Institute, Theodor-Heuss-Allee 25, 6000 Frankfurt am Main 97, F.R.G.



0021-891X/88 $03.00 + .12 

distribution of the potential and current in the electrode and, thus, on both effectivity and selectivity of the electrochemical reactor.

Cylindrical electrochemical reactors containing dimensionally stable electrodes have been proposed for indirect electrosyntheses [1]. In this case, the useful species is generated at a large cylindrical electrode, being reconverted only partially at the thin central wire electrode since its area is much smaller. At the same time, at the central electrode, a secondary reaction takes place lowering the current efficiency of the unwanted reconversion. Thus an undivided cell offering an appreciable cell voltage decrease and simplified constructive features can be applied. Since the central electrode experiences high current densities, when designing such units there is a need to take account of the distribution of the current density caused by the resistance of the metal phase. A cylindrical geometry is also useful in equipment for protection against corrosion and for metal plating on tubes or wires. Some theoretical evaluation of such systems has been undertaken [2–13], but little experimentation has been performed [2, 8, 10] for verifying the proposed models.

In this work, the current distribution along a wire electrode has been measured using two methods: (a) a reactor with a segmented counterelectrode, and (b) a bi-electrode probe. The evolution of oxygen and hydrogen from acid and alkaline solutions of different concentrations have been used as test reactions over a wide current density range. A mathematical model assuming an axial isopotential of the electrolyte was employed, the experimental results being compared with those theoretically predicted.

## 2. Mathematical model

Figure 1 shows schematically a cylindrical rod electrode (length $L$, radius $r_e$) fed at its lower end ($x = 0$); a charge balance for the region $x$, $x + dx$ is:

$$I_m(x) = I_m(x + dx) + \bar{i}[\eta(x)]\,2\pi r_e\,dx \qquad (1)$$

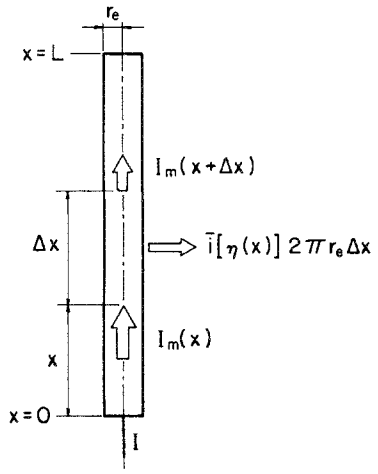


Fig. 1. Geometry of the model.

Introducing

$$i_m(x) = \frac{I_m(x)}{\pi r_e^2} \qquad (2a)$$

and

$$i_e = \frac{I}{\pi r_e^2} \qquad (2b)$$

and

$$A_s = \frac{\text{electrode surface}}{\text{electrode volume}} = \frac{2}{r_e} \qquad (3)$$

into Equation 1 and rearranging yields the differential equation

$$\frac{di_m(x)}{dx} = -A_s i[\eta(x)] \qquad (4)$$

Ohm's law for the metal phase is

$$\frac{d\phi_m(x)}{dx} = -\varrho_m i_m(x) \qquad (5)$$

Differentiating Equation 5 with respect to $x$, and introducing Equation 4 yields

$$\frac{d^2\phi_m(x)}{dx^2} = \varrho_m A_s i[\eta(x)] \qquad (6)$$

Defining the overvoltage, considering the electrolyte as being axially equipotential and neglecting the changes of $E_0$ with $x$

$$\eta(x) = \phi_m(x) - \phi_s - E_0$$

yields, by introducing into Equation 6,

$$\frac{d^2\eta(x)}{dx^2} = \varrho_m A_s i[\eta(x)] \qquad (7)$$

with the following boundary conditions:

$$x = 0, \quad \eta = \eta(0) \qquad (8a)$$

and

$$\left(\frac{d\eta}{dx}\right)_{x=0} = -\varrho_m i_e \qquad (8b)$$

Further boundary conditions are

$$x = L, \quad \eta = \eta(L) \qquad (9a)$$

and

$$\left(\frac{d\eta}{dx}\right)_{x=L} = 0 \qquad (9b)$$

Assuming a charge-transfer controlled electrode reaction yields

$$\frac{d^2\eta}{dx^2} = \varrho_m A_s i_0 \exp[b\eta(x)] \qquad (10)$$

with

$$b = \frac{\alpha_c v_e F}{RT} \qquad (10a)$$

Solving Equation 10 taking account of Equations 8a

and 8b gives

$$\eta(x) = \eta(0) - \frac{2}{b} \ln \frac{\cos [B(1 - x/L)]}{\cos (B)} \quad (11)$$

where $B$ is an integration constant determined by the following implicit equation:

$$B = L \left\{ \frac{A_s \varrho_m i_0 b}{2} \exp [b\eta(0)] \right\}^{1/2} \cos (B) \quad (12)$$

Equation 11 represents the overvoltage distribution on the electrode. By introducing Equation 11 into the simplified (large $\eta$) Butler–Volmer Equation

$$i(x) = i_0 \exp [b\eta(0)] \left\{ \frac{\cos (B)}{\cos B(1 - x/L)} \right\}^2 \quad (13)$$

gives the current density distribution.

Equation 13 states that the current density at a certain internal point of the electrode equals the current density at the feeder ($x = 0$) multiplied by a factor lower than one, which depends upon both the position at the electrode and the constant $B$.

To determine the total current ($I$) entering the electrode, the following expression can be used

$$I = i_0 \exp [b\eta(0)] 2\pi r_e L \frac{\sin (2B)}{2B} \quad (14)$$

obtained by introducing Equation 13 into the integral of Equation 4, rearranging and taking Equation 2b into consideration.

According to Equation 14, the total current, $I$, is the product of three factors: (a) the current density at $x = 0$ of the wire electrode; (b) the electrode surface area, and (c) a factor, lower than one, accounting for the effect of the resistance of the wire electrode on the current and potential distribution.

The electrode effectiveness factor, $\gamma$, is defined as the ratio of the observed current to the maximum current which would be obtained at an electrode of zero resistivity. The maximum current is given by the product of the two first factors mentioned above. Hence,

$$\gamma = \frac{\sin (2B)}{2B} \quad (15)$$

The effectiveness factor is a function of the dimensionless constant $B$ only, which (according to Equation 12) depends upon the geometry of the electrode, the resistivity of the metal phase, the kinetic parameters of the reaction considered, and the local overvoltage at the electrode entrance. By analogy to the concept of the Wagner number [14], being defined as the ratio of polarization and electrolyte resistance, a modified Wagner number can be defined accounting for the influence of the electrode resistance on the current density distribution.

$$Wa^*(x) = \frac{R_p(x)}{R_m} \quad (16)$$

where $R_p$ is the polarization resistance and $R_m$ is the resistance of the wire electrode which are defined by:

$$R_p(x) = \left(\frac{d\eta}{dI}\right)_x = \frac{1}{2\pi r_e L} \left(\frac{d}{di}\right)_x \quad (17)$$

and

$$R_m = \frac{\varrho_m L}{\pi r_e^2} \quad (18)$$

By introducing Equations 17 and 18 into Equation 16,

$$Wa^*(x) = \frac{1}{\left(\frac{di}{d\eta}\right)_x \varrho_m L^2 A_s} \quad (19)$$

Taking the derivative of the Butler–Volmer Equation with respect to $\eta$, introducing the result into Equation 19, and solving at $x = 0$,

$$Wa^*(0) = \frac{1}{i_0 \exp [b\eta(0)] b \varrho_m L^2 A_s} \quad (20)$$

Introducing Equation 20 into Equation 12,

$$B = \left[\frac{1}{2Wa^*(0)}\right]^{1/2} \cos (B) \quad (21)$$

Equation 25 states that $B$ and, hence, the effectiveness factor, depends exclusively on the modified Wagner number (defined in Equation 16) taken at the end of the electrode where the current enters.

In this way, all parameters influencing the current distribution are combined in a single dimensionless variable similar to that used in current distribution problems for other systems.

## 3. Experimental details

### 3.1. *Reactor with a segmented counterelectrode*

Figure 2 depicts schematically the equipment employed and the electrolyte flow.

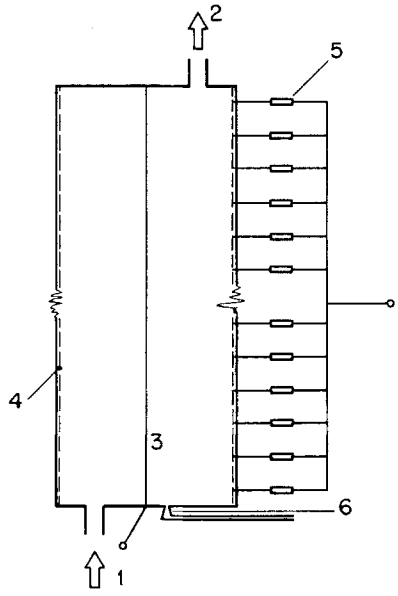


Fig. 2. Scheme of the segmented counterelectrode reactor. 1, Electrolyte inlet; 2, electrolyte outlet; 3, working electrode; 4, counterelectrode; 5, resistance; 6, Luggin capillary.

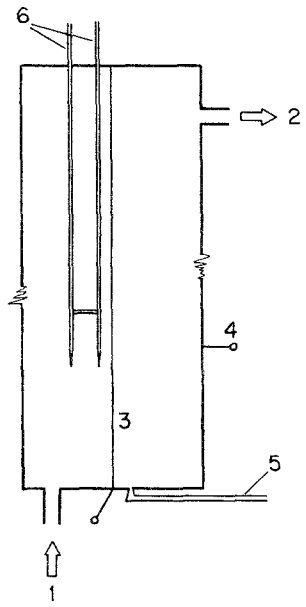


Fig. 3. Scheme of the bi-electrode probe reactor. 1, Electrolyte inlet; 2, electrolyte outlet; 3, working electrode; 4, counterelectrode; 5, Luggin capillary; 6, bi-probe.

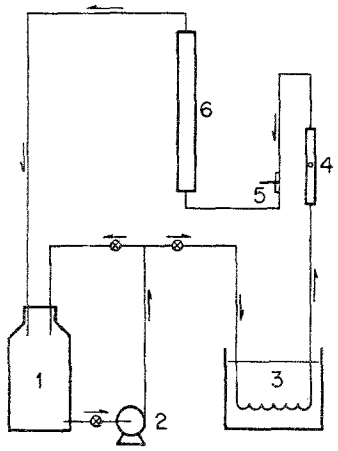


Fig. 4. Scheme of the electrolyte circulation system. 1, Reservoir; 2, pump; 3, thermostat; 4, flow meter; 5, thermometer; 6, electrochemical reactor.

The cylindrical reactor was made of acrylic material, with a 44.65 mm internal diameter and a 3.25 mm thickness. The working electrode was a Pt wire, 0.2 mm diameter and 600 mm long, centrally positioned. The segmented counterelectrode was made of 40 304 stainless steel rings, 41.35 mm internal diameter, 1.5 mm thick and 14 mm high, each ring being separated by an O-ring approximately 1 mm thick. The external ring face was covered with a chloroform-dissolved acrylic material in order to make it non-conductive. Stainless steel bolts passed through the reactor wall, pressing the ring and thus ensuring electric contact. External resistances for each electrode segment were used to measure the current distribution (see Fig. 2). Two values of the external resistance were used, 4.7 Ω and 0.09 Ω, both at 0.5 W.

As reference, a saturated calomel electrode was used, connected to a Luggin capillary located at 6.35 mm from the working electrode.

### 3.2. *Reactor with bi-electrode probe*

Figure 3 shows schematically the reactor employed. The electrolyte was caused to flow upwards, leaving the reactor through an overflow placed at 500 mm from the bottom, which thus defined the reactor length. The working electrode, made of a 0.2 mm diameter Pt wire, was centrally located, being electrically fed at its lower end. The reactor casing, a welded 304 stainless steel pipe having a 98 mm internal diameter and a 1.65 mm thickness, was used as counterelectrode.

The working electrode potential was measured at the lower end, using a saturated calomel electrode probe positioned at 8 mm from the center of the reactor.

To measure the current distribution along the Pt wire, a bi-probe was built using two glass tubes (5 mm internal diameter and 650 mm long) ending in capillary tips with a 1.7 mm external diameter. The spacing between the centerlines of the capillaries was 28.65 mm. The inner capillary was positioned at 14.90 mm from the center of the reactor. Each tube of the bi-probe was connected through small latex tubing to saturated calomel reference electrodes.

The bi-probe passed through the reactor top cover, being internally guided in the reactor by a cross support resting on the casing, thus allowing positioning at any desired height.

In both reactors, the current feed and the potential control were effected at the lower end so as to minimize the effect of the bubbles, produced by the reactions under study, on the electrolyte resistance.

The reactors were mounted in the circuit schematically shown in Fig. 4. The electrolyte was only circulated to maintain a constant temperature at a preset value. All experiments were performed under potentiostatic control.

### 3.3. *Test reactions and reagents employed*

Oxygen evolution from 0.5 M sulphuric acid solution and hydrogen generation from 0.1 M and 1 M NaOH solutions were used as test reactions. The solutions were prepared using analytical grade chemicals.

Kinetic parameters for the electrochemical reactions under study, at the same operating conditions, were obtained using a conventional potentiostatic arrangement. A portion of the Pt wire employed in the other two reactors was used as the working electrode with the following characteristics: 0.2 mm diameter and 18.8 mm long. For this electrode, the effect of the resistance of the wire on the current distribution can be neglected. A 304 stainless steel tube (95 mm internal diameter, 3.2 mm thick and 93.7 mm high) was used as the counterelectrode. When performing the experiments, the cell was immersed in a thermostatic bath.

Table 1 shows the exchange current densities and charge transfer coefficients obtained as well as the resistivity data.

*Table 1. Values of the kinetic parameters and resistivity data*

| | *Solution* | | |
|---|---|---|---|
| | *$H_2SO_4$ 0.5 M (25° C)* | *NaOH 1 M (30° C)* | *NaOH 0.1 M (30° C)* |
| $O_2$ evolution | $\alpha_c v_e = 0.6$<br>$i_0 = 7.95 \times 10^{-10}$ A cm$^{-2}$ | | |
| $H_2$ evolution | | $\alpha_c v_e = 0.48$<br>$i_0 = 2.09 \times 10^{-4}$ A cm$^{-2}$ | $\alpha_c v_e = 0.42$<br>$i_0 = 2.08 \times 10^{-4}$ A cm$^{-2}$ |
| Resistivity of the solution (Ω cm) | 5 | 5.26 | 44.05 |
| Platinum resistivity ($\mu\Omega$ cm) | 10.78 (25° C) | | 10.98 (30° C) |

### 3.4. *Data processing*

The current distribution of the reactor equipped with a segmented counterelectrode was determined by measuring the ohmic drop in the corresponding resistance; the average current density for each segment was calculated by dividing the current by the corresponding area of the working wire electrode.

During the experiments with the reactor having a bi-probe, the ohmic drop in the electrolyte was experimentally measured between its two capillaries, at different heights. Knowing the resistance of the solution in this portion, the corresponding current density was calculated.

At each experiment, the overvoltage at the lower end of the working electrodes was determined by

$$\eta_{exp}(0) = \Delta V - E_0 - \varrho_s r_e i_{exp}(0) \ln \frac{r_r}{r_e} \quad (22)$$

During each experiment, the total current passing through the reactor was measured.

The experimental results were compared with theoretical data calculated from the model. The comparison was made in two different ways: firstly, the overvoltage, $\eta_{th}(0)$, that must be applied to the working electrode at $x = 0$ in order to achieve the measured total current was computed using the model. This value was then compared with the experimental overvoltage determined according to Equation 22, the error being calculated by:

$$E = \frac{|\eta_{exp}(0) - \eta_{th}(0)|}{\eta_{th}(0)} 100\% \quad (23)$$

Secondly, for the measured total current, the theoretical current density distribution, $i_{th}(x)$, according to Equation 13 was computed using the model and compared with the experimental value.

For calculation of the current density distribution, the theoretical $\eta_{th}(0)$ value, obtained with the total experimental current, was used along with Equation 13. The agreement was checked by the mean relative deviation, $\bar{\delta}_r$, defined as:

$$\bar{\delta}_r = \frac{1}{N} \sum_{i=1}^{N} \frac{|i_{exp}(x_i) - i_{th}(x_i)|}{i_{th}(x_i)} \quad (24)$$

## 4. Results and discussion

### 4.1. *Experiments with the segmented counterelectrode reactor*

Figure 5 shows the experimental current densities as a function of position for different total currents. Hydrogen evolution from 1 M NaOH solution at 30° C was used as the test reaction. The resistors connected to each ring composing the segmented counterelectrode had a resistance 0.09 Ω. In each case, the full line represents the theoretical curve. There is a close agreement between experimental and theoretical results, the agreement being better for lower values of total current.

Table 2 summarizes these results; when analyzing column 6, a high $E$ value can be observed mainly due to the fact that when using Equation 22 to estimate $\eta_{exp}(0)$, a value of $i_{exp}(0)$ obtained by extrapolation at $x = 0$ of the respective experimental values was employed, this being a rather inaccurate procedure due to the high slope of the curves in this portion. Such difficulty was not observed in the experiments reported under Section 4.2.

For the same value of external resistance, Fig. 6 shows some typical results obtained for hydrogen evolution from 0.1 M NaOH solution at 30° C. At the same total current as in the previous case a greater deviation of the experimental results from the model was obtained. It must be noted, however, that the experimental current density distribution is more uniform than predicted.

Figure 7 shows some typical current distribution

*Table 2. Review of the results obtained with the segmented counter-electrode reactor* (R = *0.09 Ω; electrolyte: NaOH 1 M;* T = *30° C*)

| *Fig. no.* | *Curve* | I (*A*) | $\eta_{exp}(0)$ (*V*) | $\eta_{th}(0)$ (*V*) | E (%) | $\bar{\delta}_r$ |
|---|---|---|---|---|---|---|
| 5 | a | 0.174 | 0.450 | 0.366 | 22.95 | 0.1412 |
| | b | 0.271 | 0.500 | 0.411 | 21.65 | 0.1439 |
| | c | 0.392 | 0.535 | 0.449 | 19.15 | 0.2852 |
| | d | 0.486 | 0.550 | 0.472 | 16.53 | 0.4128 |
| | e | 0.639 | 0.558 | 0.502 | 11.16 | 0.6004 |
| | f | 0.727 | 0.585 | 0.515 | 13.59 | 0.6691 |

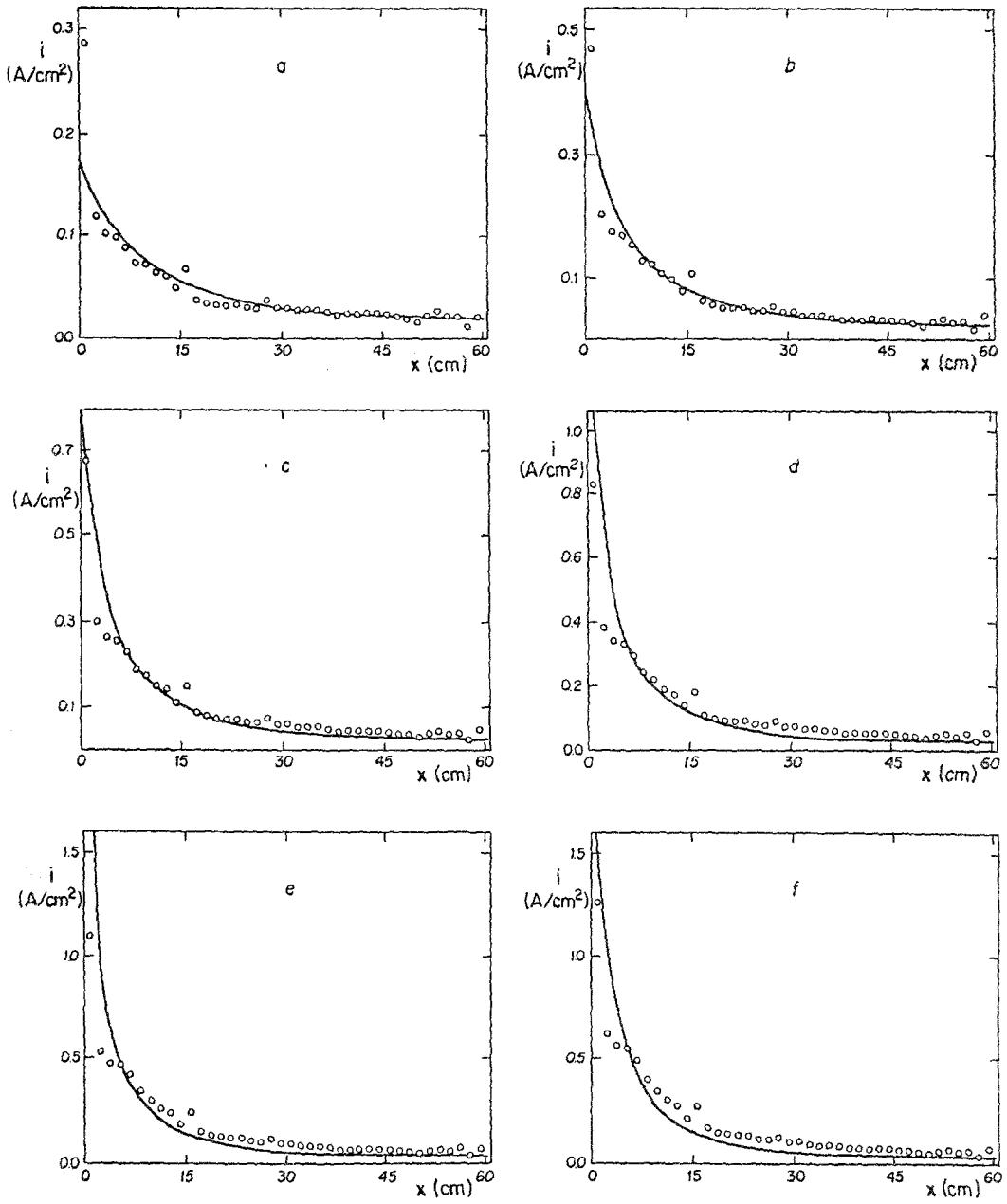


Fig. 5. Experimental and theoretical (——) current distributions for hydrogen evolution. Segmented counterelectrode method; $R$: 0.09 Ω; [NaOH] = 1 M; $T$ = 30° C; (a) 0.174 A; (b) 0.271 A; (c) 0.392 A; (d) 0.486 A; (e) 0.639 A; (f) 0.727 A.

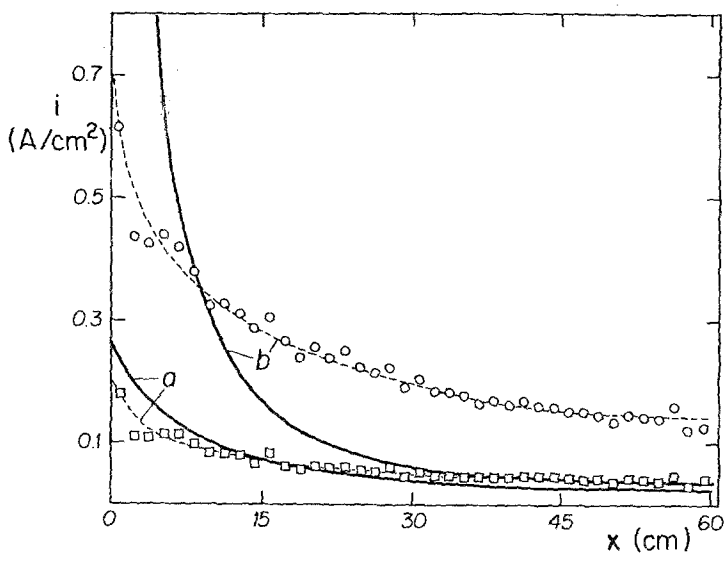


Fig. 6. Experimental (- - -) and theoretical (——) current distribution for hydrogen evolution. Segmented counterelectrode method; $R$ = 0.09 Ω; [NaOH] = 0.1 M; $T$ = 30° C; (a) 0.232 A; (b) 0.896 A.

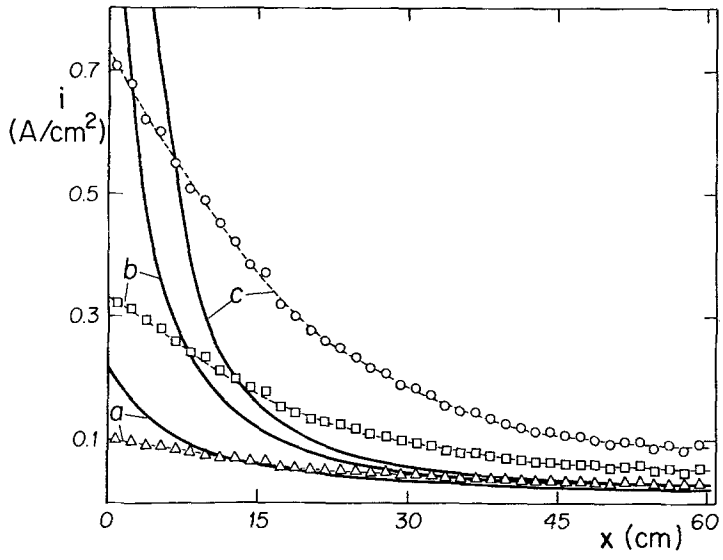


Fig. 7. Experimental (– – –) and theoretical (——) current distribution for hydrogen evolution. Segmented counterelectrode method; $R = 4.7\,\Omega$; [NaOH] = 1 M; $T = 30°\,C$; (a) 0.194 A; (b) 0.486 A; (c) 0.978 A.

curves obtained with hydrogen evolution from 1 M NaOH solution at 30° C; the external resistance attached to each ring being 4.7 Ω. By comparing these curves with those in Fig. 5 – for the same total current – a higher deviation is observed. The experimental distribution, however, is more uniform than the theoretical one, corresponding to an increased effectiveness factor.

Figure 8 summarizes the results obtained; the mean relative deviation, $\bar{\delta}_r$ (defined by Equation 24) was represented as a function of the dimensionless variable $Wa^*_{th}(0)$, given by Equation 20 calculated using $\eta_{th}(0)$.

The curve a in Fig. 8 corresponds to the results included in Fig. 5. It can be concluded that, for solutions with a high electrical conductivity – such as 1 M NaOH – the agreement of the experimental results with those given by the model is excellent when the Wagner number calculated at $x = 0$ is greater than $15 \times 10^{-3}$.

In the same figure, the points ▽ in curve b correspond to hydrogen evolution from 1 M NaOH at 30° C; some of these experiments were reported in Fig. 7, while the points ● were obtained for oxygen evolution from 0.5 M $H_2SO_4$ solution at 25° C. In both cases, the external resistance at each ring was 4.7 Ω. As both solutions have approximately the same resistivity (see Table 1) the agreement between the experimental and theoretical results is the same. The comparison of curves a and b illustrates the effect of the external resistors mounted to each ring on the current distribution of the cell.

For the curves a and b, the resistance of the solution phase between the working and the counterelectrode can be calculated on the basis of the electrical parameters and dimensions already given. A value of about 2.98 Ω is obtained. This shows that the higher value of 4.7 Ω of the external resistance alters the current distribution significantly and makes it more uniform.

In Fig. 8, the points ○ correspond to hydrogen generation from 0.1 M NaOH at 30° C with an external 0.09 Ω resistance, some of these experiments being included in Fig. 6. The points ▽ correspond to the same system but with external 4.7 Ω resistors. No discrepancy is observed between both experimental sets. This may be explained by considering that this dilute solution has an electrolyte resistance of 24.92 Ω. This value is significantly higher than that of the

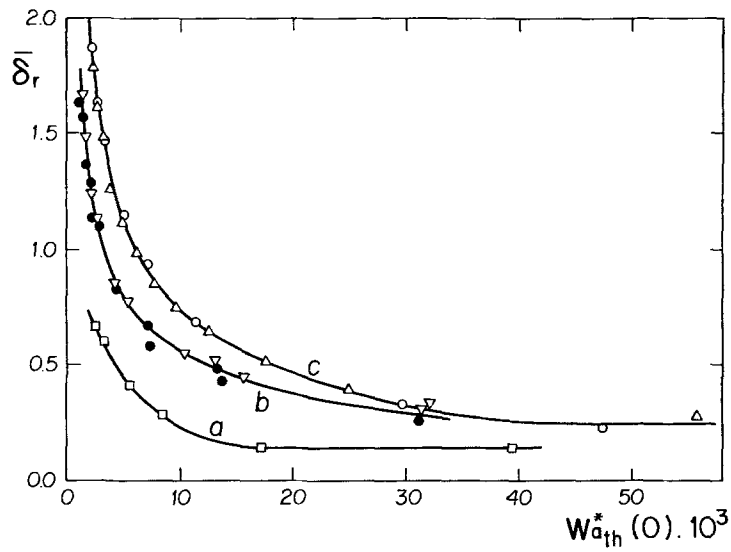


Fig. 8. $\bar{\delta}_r$ as a function of the modified Wagner number. Segmented counterelectrode method. (a) $R = 0.09\,\Omega$, $H_2$ evolution, [NaOH] = 1 M, $T = 30°\,C$; (b) $R = 4.7\,\Omega$, ▽: $H_2$ evolution, [NaOH] = 1 M, $T = 30°\,C$; ●, $O_2$ evolution, [$H_2SO_4$] = 0.5 M, $T = 25°\,C$; (c) $H_2$ evolution, [NaOH] = 0.1 M, $T = 30°\,C$; ○: $R = 0.09\,\Omega$, △: $R = 4.7\,\Omega$.

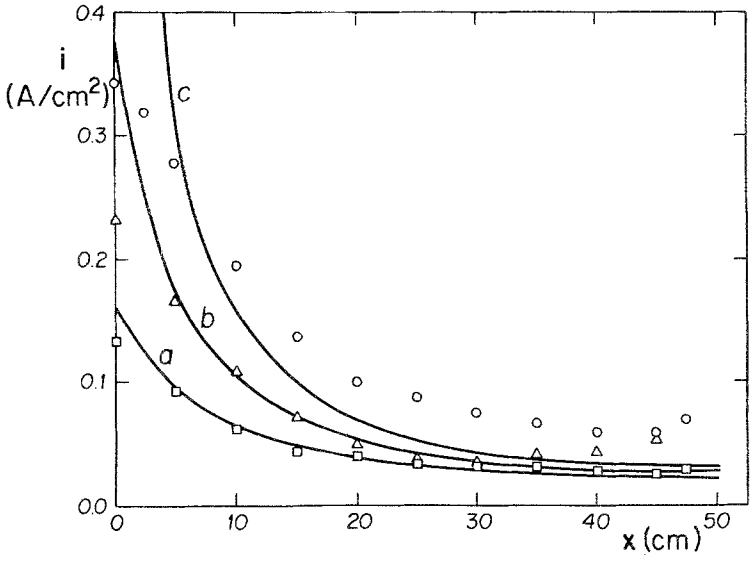


Fig. 9. Experimental and theoretical (——) current distribution for oxygen evolution. Bi-electrode probe method; $[H_2SO_4]$ = 0.5 M; $T$ = 25° C; (a) 0.147 A (□); (b) 0.234 A (△); (c) 0.396 A (○).

external resistors and, thus, dominates the resultant current distribution.

The comparison of curves a and c shows the effect of the electrolyte resistance.

### 4.2. *Experiments with the bi-probe reactor*

Figure 9 shows some typical curves obtained with this reactor. All represent the current density computed from the experimental measurements as a function of the position at the electrode for oxygen evolution from 0.5 M $H_2SO_4$ solution. For each case, the full line represents the theoretical curve. As in the previous case, it can be observed that when the electrolyte has a high conductivity the agreement between the experimental and theoretical distributions is close, improving as the total current decreases. The latter observation is obviously due to the decrease of polarization resistance with increasing current. The effect of the electrolyte resistance on the current distribution becomes more dominating making it more uniform. Table 3 summarizes the results obtained with this reactor.

When employing the bi-probe method, it is possible to determine the current density of the working electrode closer to $x = 0$ and, by using Equation 22, the applied overvoltage can be calculated. From column 6 in this table, it can be concluded that the error introduced in estimating the overvoltage at $x = 0$ is very small.

Figure 10 shows the mean relative deviation, $\bar{\delta}_r$, as a function of the dimensionless variable, $Wa^*_{th}(0)$; the points of curve b correspond to the above experiments. For the sake of comparison, the curve a in Fig. 8 is also included; corresponding to hydrogen evolution from 1 M NaOH at 30° C, employing the segmented counterelectrode method with an additional 0.09 Ω resistance connected to each ring. It can be seen that, for high modified Wagner numbers, $Wa^*_{th}(0)$, the deviations of both methods coincide approximately. For lower values of the dimensionless parameter, however, a greater discrepancy is observed in the results obtained with the bi-probe (i.e. there is a higher $\bar{\delta}_r$). This situation may be explained by taking into account that the second reactor has a greater radius than the first one; consequently, the resistance of the solution phase is higher, thereby exerting a stronger influence on the current distribution.

In Fig. 10, the full line represents the theoretical

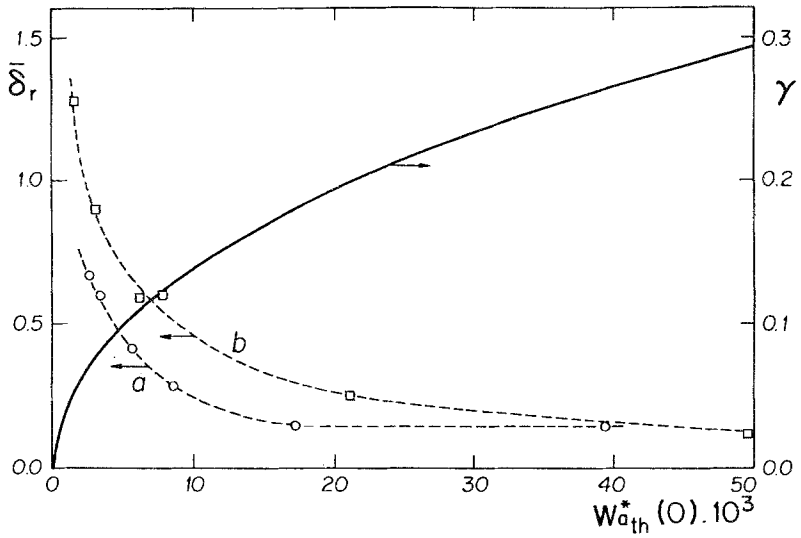


Fig. 10. $\bar{\delta}_r$ and effectiveness factor as a function of the modified Wagner number. (a) Segmented counterelectrode method, $R$ = 0.09 Ω, $H_2$ evolution, [NaOH] = 1 M, $T$ = 30° C; (b) bi-probe method, $O_2$ evolution, $[H_2SO_4]$ = 0.5 M, $T$ = 25° C. Full line (——): theoretical effectiveness factor according to Equations 18 and 25.

*Table 3. Review of the results obtained with the bi-electrode probe reactor (electrolyte: $H_2SO_4$ 0.5 M; T = 25° C)*

| *Fig. no.* | *Curve* | I (*A*) | $\eta_{exp}(0)$ (*V*) | $\eta_{th}(0)$ (*V*) | E (%) | $\delta_r$ |
|---|---|---|---|---|---|---|
| | a | 0.147 | 0.834 | 0.819 | 1.83 | 0.1228 |
| 9 | b | 0.234 | 0.862 | 0.856 | 0.70 | 0.2508 |
| | c | 0.396 | 0.892 | 0.899 | 0.78 | 0.6030 |
| | | 0.446 | 0.924 | 0.909 | 1.65 | 0.5937 |
| | | 0.645 | 0.975 | 0.940 | 3.72 | 0.9012 |
| | | 0.908 | 0.998 | 0.969 | 2.99 | 1.2812 |

effectiveness factor as a function of $Wa^*_{th}(0)$ given by Equations 15 and 21. It can be seen that the relationship between $\gamma$ and $Wa^*_{th}(0)$ is a monotonically increasing function. A reasonably large effectiveness factor is obtained only for high values of the modified Wagner number. Under these conditions, it has been shown that the model predicts quite accurate results so that it can be reliably used to design such reactors.

## 5. Conclusions

From this work, the following conclusions may be drawn:

(i) The experimental results obtained with solutions of high electrical conductivity agree reasonably well with the values predicted by the proposed model if the modified Wagner number evaluated at $x = 0$ (as defined by Equation 20) exceeds $15 \times 10^{-3}$.

(ii) When working with electrolyte solutions of higher resistivities, the behaviour of the reactor can be predicted by the model, but with a larger error.

(iii) If the resistance of the solution increases, or if an external resistance is included, a more uniform current distribution can be achieved, and the effectiveness factor increases correspondingly.

(iv) All deviations between the model and the experiments at low modified Wagner number are due to the fact that the present model neglects the influence of the electrolyte resistance. Therefore, a more sophisticated model will be reported in a further communication. For engineering purposes, however, the existing model is adequate.

## Acknowledgements

The authors would like to thank Stiftung Volkswagenwerk, Federal Republic of Germany for financial support of this work in the form of a partnership project. One of us (J.M.B.) also thanks Deutscher Akademischer Austauschdienst (DAAD) of the Federal Republic of Germany for donating some scientific equipment and DECHEMA Deutsche Gesellschaft für Chemisches Apparatewesen, Chemische Technik und Biotechnologie e.V. for acting as research project partner.

## References

[1] A. J. Bellamy and B. R. Simpson, *Chem. Ind. (Lond.)* (1981) 328.
[2] A. Weisselberg and Staff, *Trans. Electrochem. Soc.* **90** (1946) 235.
[3] C. W. Tobias and R. Wijsman, *J. Electrochem. Soc.* **100** (1953) 459.
[4] W. W. Harvey, *J. Electrochem. Soc.* **109** (1962) 638.
[5] S. Zaromb, *J. Electrochem. Soc.* **109** (1962) 912.
[6] B. E. Conway, E. Gileadi and H. G. Oswin, *Can. J. Chem.* **41** (1963) 2447.
[7] S. K. Rangarajan, M. J. Dignam and B. E. Conway, *Can. J. Chem.* **45** (1967) 422.
[8] J. Wojtowicz, L. Laliberté and B. E. Conway, *Electrochim. Acta* **13** (1968) 361.
[9] R. Alkire and R. Varjian, *J. Electrochem. Soc.* **121** (1974) 622.
[10] A. Tvarusko, *J. Electrochem. Soc.* **121** (1974) 660.
[11] P. M. Robertson, *Electrochim. Acta* **22** (1977) 411.
[12] K. Hertwig and J. Breme, *Chem. Techn. (Leipzig)* **32** (1980) 294.
[13] K. Scott, *J. Appl. Electrochem.* **13** (1983) 209.
[14] C. Wagner, *J. Electrochem. Soc.* **98** (1951) 116.